# A Novel Fully Implicit Multigrid Driven Algorithm for Unsteady Incompressible Flow Calculations

Andrey Belov, Luigi Martinelli, Antony Jameson
Princeton University, Princeton, New Jersey, USA

*Proceedings*
ECCOMAS '94

Stuttgart

September, 1994

# A Novel Fully Implicit Multigrid Driven Algorithm for Unsteady Incompressible Flow Calculations

**Andrey A. Belov, Luigi Martinelli** and **Antony Jameson** [1]

**Abstract.**

We present a new implicit algorithm for the solution of unsteady incompressible flows using the primitive variable formulation. The artificial compressibility approach is coupled with an implicit A-stable discretization of the time derivatives. The resulting non-linear system is solved at every time step by using a very efficient multigrid time stepping technique.

Results for both steady and unsteady test problems are presented. Calculations of the inviscid steady flow over a circular cylinder are presented to assess the accuracy of the spatial discretization, as well as to quantify the numerical errors introduced by the artificial dissipation. An inviscid two-dimensional flow over an accelerating cylinder is used to validate the numerical method by comparison with analytic results. Finally, computed results for a NACA0012 airfoil in pitching motion are found to be in excellent agreement with experimental data.

## 1 Nomenclature

| | |
|---|---|
| $a$ | non-dimensional location of the pitching axis, positive aft of midchord |
| $b$ | airfoil semichord |
| $c$ | airfoil chord |
| $L$ | lift force per unit span normal to free stream |
| $D$ | drag force per unit span |
| $C_l$ | lift coefficient |
| $C_d$ | drag coefficient |
| $C_p$ | pressure coefficient |
| $R$ | cylinder radius |
| $\vec{u}_{cyl}$ | cylinder velocity vector |
| $C_{d_{cyl}}$ | drag coefficient of the accelerating cylinder defined as $C_{d_{cyl}}=\frac{D}{\rho u_{cyl}^2 R}$ |
| $k_c$ | reduced frequency, $k_c = \frac{\omega b}{U_\infty}$ |
| $p$ | static pressure |
| $p_\infty$ | static pressure at the far field |
| $\rho$ | density |
| $\mathbf{R}(\mathbf{w}_{ij})$ | flux residual for the cell $ij$ |
| $\mathbf{R}^*$ | modified residual |
| $t$ | time |
| $t^*$ | pseudo-time |
| $u,v$ | Cartesian velocity components |
| $U_\infty$ | free stream velocity |
| $x_t,y_t$ | Cartesian components of the mesh velocity |
| $V_{ij}$ | volume of the cell $ij$ |
| $\mathbf{w}$ | solution vector |
| $\alpha$ | angle of attack |
| $\Delta\alpha$ | amplitude of the pitching motion |
| $\Delta t$ | implicit time step |
| $\Omega,\partial\Omega$ | control volume and its boundary |

[1] Department of Mechanical and Aerospace Engineering
Princeton University
Princeton, New Jersey 08544 U.S.A.


ECCOMAS 94.
Published in 1994 by John Wiley & Sons, Ltd.

## 2 Introduction

In the past fifteen years, several fast and accurate algorithms have been developed for solving the steady Euler and Navier-Stokes equations [1]. In particular, multigrid schemes have greatly enhanced the efficiency of both compressible and incompressible solvers [2, 3]. Currently, steady solutions to the three-dimensional Euler equations require only 20 to 50 multigrid steps. These very efficient algorithms are routinely used in industry for the analysis of steady flows on complex aerospace configurations. The increase in convergence rate is generally achieved, however, at the expense of time accuracy. On the other hand, unsteady flows are of great practical interest for a large class of complex engineering problems. For example, the computational analysis of aeroelastic phenomena requires the coupling of structural analysis with non-linear time-dependent fluid dynamics models. Similarly, the analysis of the "sea-keeping" problem requires the coupling of non-linear fluid dynamics models comprising the evolution of free-surfaces with the dynamics of floating bodies. This paper describes a novel approach for computing time-resolved, incompressible flows using the primitive variable formulation. The method is presented and validated by using the two-dimensional Euler equations. Nevertheless, the algorithm is quite general and carries over to both three-dimensional, and viscous flows.

One of the major difficulties encountered in the calculation of incompressible flows stems from the time-independent constraint imposed on the velocity field by the continuity equation. Several methods have been proposed to enforce

a solenoidal velocity field and to recouple the velocity and pressure fields. One very efficient approach, which is generally referred to as the artificial compressibility method, was introduced by Chorin [4]. Chorin's method transforms the incompressible Euler equations to an hyperbolic system by introducing, in the continuity equation, a pseudo-temporal evolution term for the pressure. Hence, the same fast algorithms originally developed for compressible flows can be applied to compute incompressible steady-state solutions. The artificial compressibility approach has been widely used by several authors. In particular, it has been succesfully applied to rotational inviscid flows by Rizzi and Eriksson [5]. More recently, the artificial compressibility method, coupled with a multigrid time stepping scheme, enabled the efficient computation of steady three-dimensional flows over ship hulls comprising free surfaces [6, 7].

In its original form, the artificial compressibility method sacrifices time accuracy. Rogers and Kwak [8], however, were able to devise a clever framework and extend the artificial compressibility approach to time resolved computations. Firstly, the time derivatives in the momentum equations are discretized at each mesh point and added to the spatial residuals. Then, an iterative procedure can be devised to solve the resulting non-linear system of equations. In effect, this iteration process is equivalent to adding pseudo-temporal terms to both the continuity and the momentum equations and driving the resulting modified system to a steady state at every time-step.

Our method builds upon similar ideas. Following Rogers and Kwak [8], we adopt a second order A-stable discretization of the time derivatives. However, in the present method, the iteration process is built upon a multigrid time stepping algorithm originally developed by Jameson [2] for the compressible Euler equations. The net result is a very efficient, implicit algorithm for simulating unsteady incompressible flows.

## 3 Governing Equations and Numerical Discretization

The flow is described by the non-linear time-dependent Euler equations without body forces. Let $p$, $\rho$, $u$, $v$ denote the pressure, density, and Cartesian velocity components, respectively. For a control volume $\Omega$ with boundary $\partial\Omega$ moving with Cartesian velocity components $x_t$ and $y_t$, the equations of motion of the fluid can be written for a stationary Cartesian coordinate system $(x,y)$ in integral vector form as

$$\mathbf{I}^{\mathbf{m}} \cdot \frac{d}{dt} \iint_{\Omega} \mathbf{w}\, dx\, dy + \oint_{\partial\Omega} (\mathbf{f}\, dy - \mathbf{g}\, dx) = \mathbf{0}. \quad (1)$$

Here $\mathbf{w}$ is the vector of flow variables

$$\mathbf{w} = \begin{Bmatrix} p \\ \rho u \\ \rho v \end{Bmatrix},$$

$\mathbf{f}$ and $\mathbf{g}$ are the Euler flux vectors

$$\mathbf{f} = \begin{Bmatrix} \rho(u - x_t) \\ \rho u(u - x_t) + p \\ \rho v(u - x_t) \end{Bmatrix}, \mathbf{g} = \begin{Bmatrix} \rho(v - y_t) \\ \rho u(v - y_t) \\ \rho v(v - y_t) + p \end{Bmatrix},$$

and $\mathbf{I}^{\mathbf{m}}$=diag[0,1,1] is a modified identity matrix which annihilates the temporal derivative of the pressure from the continuity equation.

Equation 1 is discretized using a finite-volume, cell-centered formulation yielding a set of ordinary differential equations which can be written as

$$\frac{d}{dt}(\mathbf{w}_{ij} V_{ij}) + \mathbf{R}(\mathbf{w}_{ij}) = \mathbf{0}. \quad (2)$$

Here $V_{ij}$ is the volume of the $ij$ cell and the residual $\mathbf{R}(\mathbf{w}_{ij})$ approximates the boundary integral of Equation 1. On a regular Cartesian mesh, the discretization of the convective fluxes reduces to central differencing in space. Thus a third order artificial dissipation term is added, in conservation form, to prevent odd-even decoupling [6].

Dropping the subscript $ij$ for clarity, Equation 2 can be approximated implicitly as

$$\frac{d}{dt}[\mathbf{w}^{n+1} V^{n+1}] + \mathbf{R}(\mathbf{w}^{n+1}) = \mathbf{0}, \quad (3)$$

where the superscript $n+1$ denotes the current time level $(n+1)\Delta t$. By approximating further the time derivative with a second order accurate implicit backwards difference formula, Equation 3 becomes

$$\frac{3}{2\Delta t}[\mathbf{w}^{n+1} V^{n+1}] - \frac{2}{\Delta t}[\mathbf{w}^{n} V^{n}] + \frac{1}{2\Delta t}[\mathbf{w}^{n-1} V^{n-1}] + \mathbf{R}(\mathbf{w}^{n+1}) = \mathbf{0}. \quad (4)$$

This time discretization is A-stable [9].

It is convenient at this point to define the modified residual

$$\mathbf{R}^*(\mathbf{w}) = \frac{3}{2\Delta t}[\mathbf{w}\, V^{n+1}] - \frac{2}{\Delta t}[\mathbf{w}^{n} V^{n}] + \frac{1}{2\Delta t}[\mathbf{w}^{n-1} V^{n-1}] + \mathbf{R}(\mathbf{w}).$$

Clearly, we seek a vector $\mathbf{w}$ which is the solution of $\mathbf{R}^*(\mathbf{w})=0$. Thus, we must solve a non-linear system of equations at every time step. To enhance computational efficiency the system is solved by using an iterative method. Also, if the volume of the computational cell does not change with time, we can simplify the model by dividing Equation 4 by the cell volume and by rescaling the modified residuals accordingly.

In general, an iteration process can be constructed starting from an equation of the form

$$\frac{d\mathbf{w}}{dt^*} + \mathbf{R}^*(\mathbf{w}) = \mathbf{0}, \quad (5)$$

in which $t^*$ is a fictitious *pseudo-time*. Thus, at every time step, the solution vector $\mathbf{w}$ can be obtained by computing a steady-state solution of Equation 5 through use of a multigrid time

stepping scheme. This strategy has been successfully applied to compute time resolved compressible flows [10, 11]. In the following section we discuss the coupling with the artificial compressibility method.

## 3.1 Local Preconditioning

In the limit of incompressible flow, sound waves travel infinitely fast in all directions. The disparity in the acoustic and convective speeds makes the governing system of equations ill-conditioned. Thus, a preconditioning matrix $\mathbf{Pr}$ must be introduced to render the system of equations suitable for numerical computation. More precisely, Equation 5 becomes

$$\frac{d\mathbf{w}}{dt^*} + \mathbf{Pr} \cdot \mathbf{R}^*(\mathbf{w}) = \mathbf{0}. \tag{6}$$

The simplest, symmetric form of preconditioning

$$\mathbf{Pr} = \mathbf{diag}[\Gamma^2, 1, 1]$$

is equivalent to the pseudo-compressibility method. The parameter $\Gamma$ can be chosen to optimize the rate of convergence of the iteration in pseudo-time. Since the unsteady terms enter the modified residual as source terms, the form suggested by Rizzi and Eriksson [5] can be used. In particular, we set

$$\Gamma^2 = \max(C_1, C_2(u^2 + v^2)),$$

where $C_1$=0.25 and $C_2$=1 [12].

Equation 6 is an explicit set of ordinary differential equations to be solved at each time-step. Once the iteration has reached convergence (*i.e.*, a steady-state in pseudo-time $t^*$ has been obtained), the modified residuals $\mathbf{R}^*(\mathbf{w})$ are identically zero at each mesh point, yielding the solution vector $\mathbf{w}$ at the next time level $(n+1)$. Then, the time levels in Equation 4 are shifted and a new steady-state iteration is set up. The original unsteady problem represented by Equation 2 is thus converted into a number of steady-state calculations in $t^*$.

A five-stage scheme is used to advance the solution in pseudo-time. Since the details of the pseudo-transient evolution are immaterial, standard convergence acceleration techniques can be employed. In particular, the coefficients of the multi-stage scheme are optimized for convergence. In addition, a local pseudo-time step and residual averaging are used. Moreover, a very efficient multigrid strategy originally developed by Jameson [2] for compressible flows is implemented.

## 3.2 Multigrid

The multigrid scheme is a full approximation scheme defined as follows [2, 3]. Denote the grids by a subscript $k$. Start with a time step on the finest grid $k$=1. Transfer the solution from a given grid to a coarser grid by a transfer operator $P_{k,k-1}$, so that the initial state on grid $k$ is

$$w_k^{(0)} = P_{k,k-1} w_{k-1}.$$

Then on grid $k$ the multistage time stepping scheme is reformulated as

$$w_k^{(q+1)} = w_k^{(0)} - \alpha_n \Delta t \left(R_k^{(q)} + G_k\right),$$

where the residual $R_k^{(q)}$ is evaluated from current and previous values as above. The forcing function $G_k$ is defined as the difference between the aggregated residuals transferred from grid $k-1$ and the residual recalculated on grid $k$. Thus

$$G_k = Q_{k,k-1} R\left(w_{k-1}\right) - R\left(w_k^{(0)}\right),$$

where $Q_{k,k-1}$ is another transfer operator. On the first stage the forcing term $G_k$ simply replaces the coarse grid residual by the aggregated fine grid residuals. The accumulated correction on a coarser grid is transferred to the next higher grid by an interpolation operator $I_{k-1,k}$ so that the solution on grid $k-1$ is updated by the formula

$$w_{k-1}^{new} = w_{k-1} + I_{k-1,k}\left(w_k - w_k^{(0)}\right).$$

The whole set of grids is traversed in a $W$-cycle in which time steps are only performed when moving down the cycle.

## 3.3 Boundary Conditions

The Euler formulation only requires the flow tangency condition at all solid boundaries. Therefore the normal component of the momentum flux is set to zero at the solid surface. In a cell-centered formulation the pressure at the wall must be computed from the values at interior cells. From the conservation equation of normal momentum, we first compute the pressure gradient normal to the wall ( $p_n$) at the cell-centers adjacent to the solid surface. This value of $p_n$ is then used to extrapolate the pressure at the solid boundary.

The outer boundary of the computational domain is extended from the body to a distance equal to approximately 200 chord lengths. Approximate, non-reflective far-field boundary conditions, originally used for steady problems in [6], are reformulated for a moving mesh. Depending on the normal component of the relative velocity vector at the outer boundary, either inflow or outflow conditions are imposed. The variables are assumed to be equal to the free stream values at the inflow, while they are extrapolated from the interior at the outflow.

# 4 Numerical Results

The steady-state solver is the core of our implicit method. Accordingly, both steady and unsteady flow problems are considered in order to assess the accuracy and efficiency of the proposed algorithm. Calculations of the inviscid flow over a stationary and an accelerating cylinder provided a severe test for the present method.

## 4.1 Steady Flow Calculations

A uniform, inviscid, two-dimensional flow over a fixed cylinder is calculated using three O-meshes with $80 \times 16$, $160 \times 32$, and $320 \times 64$ grid points. The pressure coefficient distribution on the surface of the cylinder for the $80 \times 16$ grid is presented in Figure 1 and compared with the potential flow solution. Minor losses of base pressure at the downstream side are indicated by the value of the drag coefficient, which is obtained by integrating the pressure coefficient distribution over the surface of the cylinder. A logarithmic plot of the computed drag coefficient versus the number of grid points used is presented in Figure 2. This plot shows that the error becomes vanishingly small as the grid is refined. Notice that an eightfold reduction in the computed drag coefficient is obtained every time the number of points in each coordinate direction is doubled. This is consistent with the third-order accurate artificial dissipation model used, and confirms that the scheme is at least second-order accurate. The computed $C_d$ was found to be less than 0.006 for all grids, and less than 0.0001 for the finest grid used.

A steady inviscid flow over the NACA0012 airfoil at an angle of attack is considered next. The inner part of the $128 \times 32$ O-mesh used is illustrated in Figure 3. The computed $C_l - \alpha$ curve is shown in Figure 4. It can be seen that the Euler solution is in excellent agreement with potential flow results. The computed drag coefficient is less than 10 drag counts for the entire range of angles of attack considered. Figure 5 represents the convergence history of the computed lift coefficient. The corresponding convergence histories for the drag coefficient, and the maximum $\delta p/\delta t^*$ residual are shown in Figure 6. These convergence plots demonstrate that a fully converged result is obtained in approximately 50 multigrid cycles.

## 4.2 Unsteady Test Problems

The unsteady inviscid flow over a cylinder accelerating with nondimensional velocity

$$\vec{u}_{cyl} = -t \cdot \vec{i},$$

is considered next. Here $\vec{i}$ is a unit vector in the $x$-direction, and $t$ is the physical time. The fluid in the far field is assumed to be stationary. An analytical solution for this problem exists, and it can be found in [13]. The drag coefficient of a cylinder due to the apparent mass effect, nondimensionalized by the instantaneous cylinder velocity and its diameter, is given by

$$C_{d_{cyl}} = \frac{\pi}{2}.$$

Three of the calculations are performed to establish grid independent results and to assess time accuracy. Two sets of calculations are carried out using a $80 \times 16$ O-mesh rigidly attached to the cylinder. The time steps are taken as $\Delta t$=.25, and $\Delta t$=.125 respectively. The third calculation is carried out on a finer $320 \times 64$ mesh with $\Delta t$=.25. In all cases, full convergence of the iteration in pseudo-time is achieved at each time-step using approximately 100 multigrid cycles. Figure 7 shows that, for all three cases, the computed drag coefficient lies on the theoretical curve as the cylinder moves a distance equal to one diameter in the negative $x$-direction. Differences in the fourth significant digit can only be appreciated on a plot with an extremely magnified scale, which is presented in Figure 8. Note that even on this scale, the results for the finest grid are virtually indistinguishable from the theoretical solution. The pressure coefficient and velocity distributions on the surface of the moving cylinder are compared with the theoretical solution in Figures 9 and 10, respectively. Again, the results correspond to a translation of the cylinder equal to one diameter. Excellent agreement is achieved even for the coarsest $80 \times 16$ grid. Instantaneous streamlines of the flow field relative to the cylinder are shown in Figure 11. A detail of the corresponding vector flow field in the vicinity of the rear stagnation point is presented in Figure 12 for the $80 \times 16$ grid. Figure 12 indicates that there is no recirculation pattern induced by the artificial dissipation, and that the flow stagnates at the theoretical stagnation point.

Results for the flow over the NACA0012 airfoil in pitching motion are discussed next. A uniform free stream is impinging on the airfoil which is pitching about an axis located at $a = -0.13$ with reduced frequency $k_c$=0.4. The amplitude of the motion is chosen to be $\Delta\alpha = \pm 6.7$ degrees. This set of parameters corresponds to the experimental conditions reported in reference [14]. As before, three Euler calculations were performed. The two calculations on the $80 \times 16$ and the $160 \times 32$ mesh use 24 time-steps per pitching cycle. The last calculation on $80 \times 16$ mesh uses 48 time-steps per pitching cycle. The initial angle of attack is set to zero and, after the third complete cycle of pitching motion, the coefficient of lift is found to achieve its limiting behavior. A plot of the coefficient of lift versus the angle of attack computed during the third pitching cycle is presented in Figure 13. The theoretical predictions are graphed using a solid line, while the experimental data are shown with a dashed line. Excellent agreement with the experiment is clearly indicated for all our calculations. The consistency of the three Euler solutions obtained with different grid and time resolution suggests that 24 steps are sufficient to resolve the complete pitching cycle on a $80 \times 16$ grid.

# 5 Conclusions

The tests performed so far strongly indicate that the new algorithm yields efficient and accurate solutions to unsteady incompressible flow problems. The fully implicit A-stable time discretization allows the use of a time-step determined only by the physical time scale of the problem. Coupling of the artificial compressibility approach with the multigrid acceleration technique insures that a fully converged solution is achieved on each time-step in less than 100 multigrid cycles. This corresponds to a CPU time of $5 \times 10^{-2}$ sec. per time-

step per mesh point, on a single processor of a Convex C220 computer. Extensions of the present method to viscous flows are currently under way.

## REFERENCES


[1] Jameson, A., "Successes and challenges in computational aerodynamics," *AIAA paper 87-1184-CP*, AIAA 8th Computational Fluid Dynamics Conference, Honolulu, Hawaii, 1987.

[2] Jameson, A., "Solution of the Euler Equations by a Multigrid Method," Applied Mathematics and Computation, Vol. 13, pp. 327-356, 1983.

[3] Jameson, A., "Multigrid algorithms for compressible flow calculations," In W. Hackbusch and U. Trottenberg, editors, *Lecture Notes in Mathematics, Vol. 1228*, pages 166–201. Proceedings of the 2nd European Conference on Multigrid Methods, Cologne, 1985, Springer-Verlag, 1986.

[4] Chorin, A.J., "A Numerical Method for Solving Incompressible Viscous Flow Problems," Journal of Computational Physics, Vol. 2, pp. 12-26, 1967.

[5] Rizzi, A. and Eriksson L.-E., "Computation of Inviscid Incompressible Flow with Rotation," Journal of Fluid Mechanics, Vol. 153, pp. 275-312, 1985.

[6] Farmer, J., Martinelli, L. and Jameson, A., "Fast Multigrid Method for Solving Incompressible Hydrodynamic Problems with Free Surfaces," AIAA Journal, Vol. 32, No. 6, pp. 1175-1182, June 1994.

[7] Farmer, J., Martinelli, L. and Jameson, A., "A Fast Multigrid Method for Solving the Nonlinear Ship Wave Problem with a Free Surface," presented at the 6th International Conference on Numerical Ship Hydrodynamics, Iowa City, August 1993.

[8] Rogers, S.E. and Kwak, D., "Upwind Differencing Scheme for the Time-Accurate Incompressible Navier-Stokes Equations," AIAA Journal, Vol. 28, No. 2, pp. 253-262, February 1990.

[9] Jeltsch, R., "Stability on the Imaginary Axis and A Stability of Linear Multistep Methods," BIT, Vol. 18, 1978, pp. 170-174 .

[10] Jameson, A., "Time Dependent Calculations Using Multigrid, with Applications to Unsteady Flows Past Airfoils and Wings," AIAA Paper 91-1596, June 1991.

[11] Alonso, J.J. and Jameson, A., "Fully–Implicit Time–Marching Aeroelastic Solutions," AIAA Paper 94-0056, January 1994.

[12] Dreyer, J., "Finite Volume Solutions to the Unsteady Incompressible Euler Equations on Unstructured Triangular Meshes," M.S. Thesis, MAE Dept., Princeton University, 1990.

[13] Landau, L.D. and Lifshitz, E.M.,"Fluid Mechanics," Pergamon Press, 1987.

[14] Halfman, R. L., "Experimental Aerodynamic Derivatives of a Sinusoidally Oscillating Airfoil in Two-Dimensional Flow," NACA Report 1108, 1952.


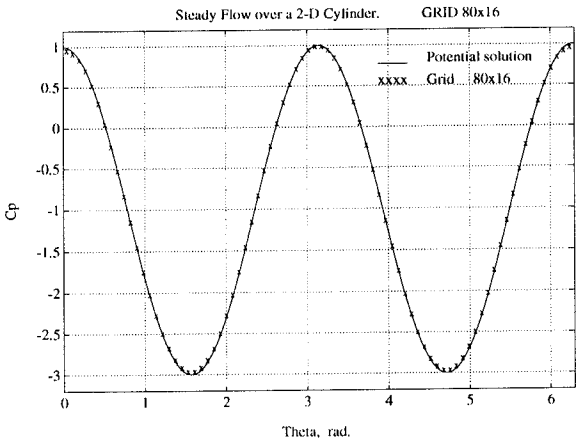


**Figure 1.** Pressure Coefficient Distribution over the Surface of a Cylinder, Grid 80 × 16.

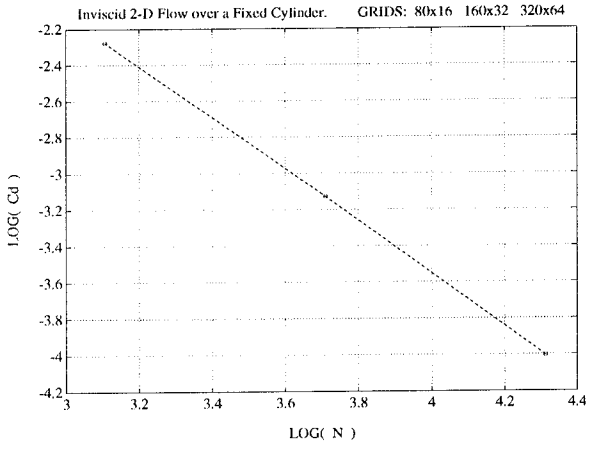


**Figure 2.** Grid Refinement Study of the Computed Drag Coefficient.

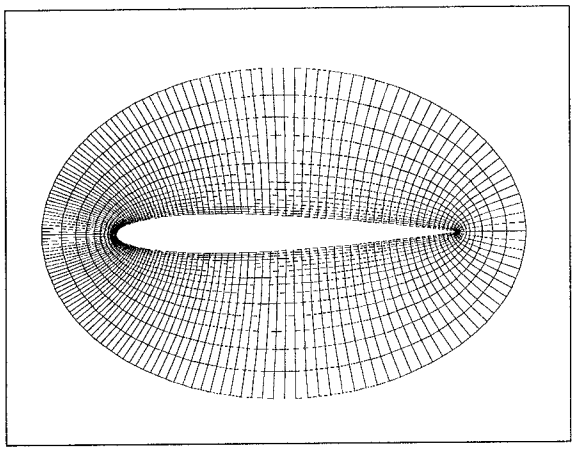

**Figure 3.** Inner part of the 128 × 32 O-Mesh.

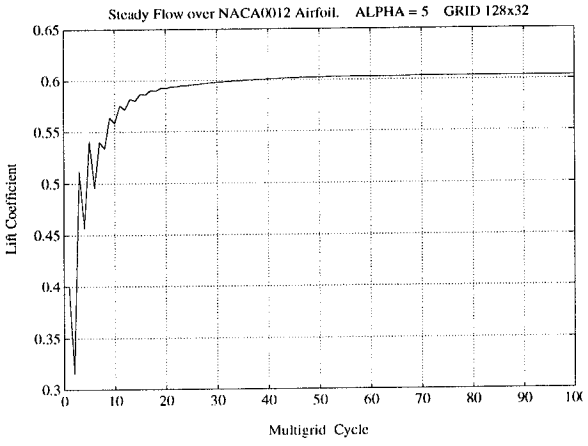


**Figure 5.** Convergence History as Measured by the Lift Coefficient – NACA0012 at $\alpha$=5°.

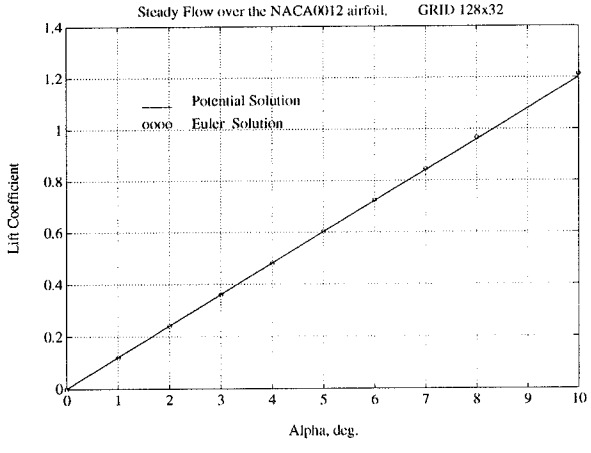


**Figure 4.** Computed $C_l - \alpha$ curve – NACA0012 Airfoil

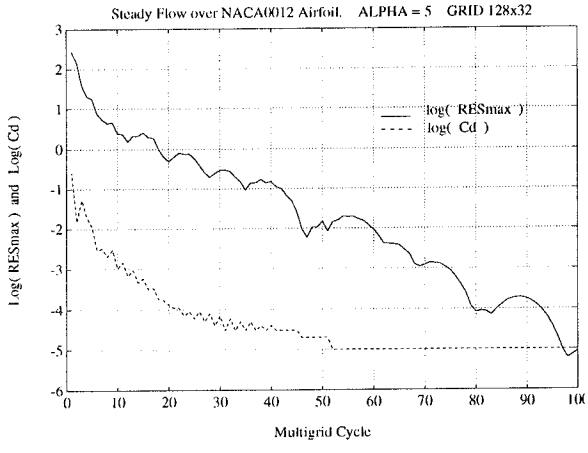


**Figure 6.** Convergence History as Measured by the Drag Coefficient and the Maximum Continuity Residual.

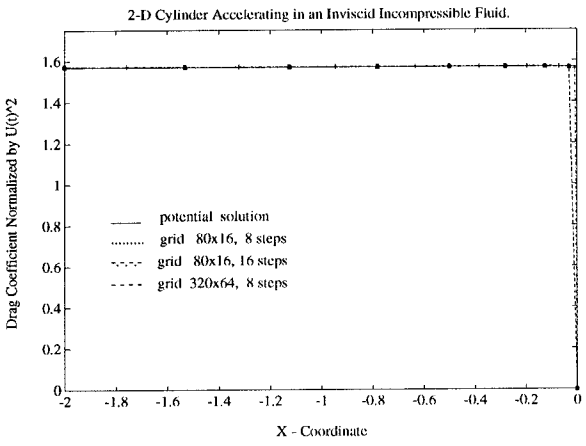


**Figure 7.** Drag Coefficient of the Uniformly Accelerating Cylinder.

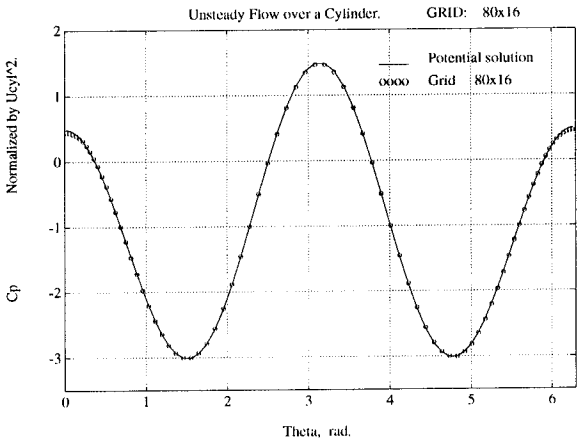


**Figure 9.** Pressure Coefficient Distribution on the Accelerating Cylinder, $x = -2R$.

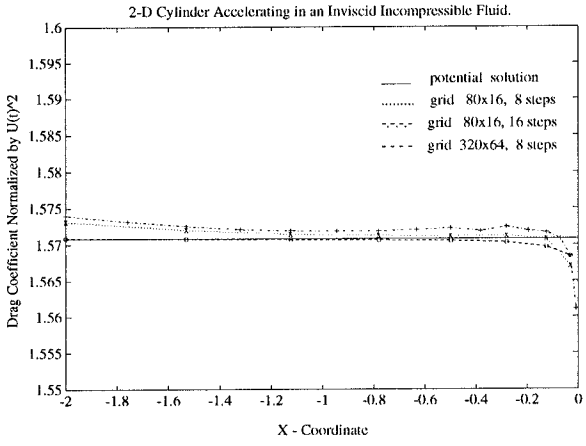


**Figure 8.** Drag Coefficient of the Uniformly Accelerating Cylinder, Magnified Scale.

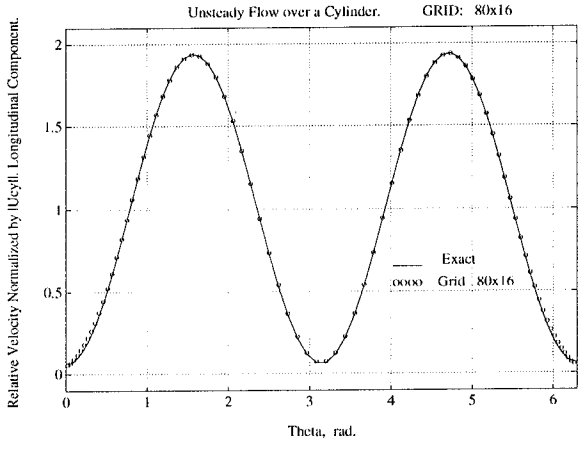


**Figure 10.** Surface Distribution of the $x$-Component of Velocity, $x = -2R$.

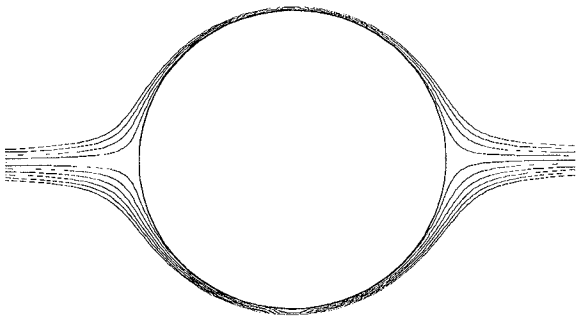

**Figure 11.** Instantaneous Streamlines of the Flow Field Relative to the Cylinder.

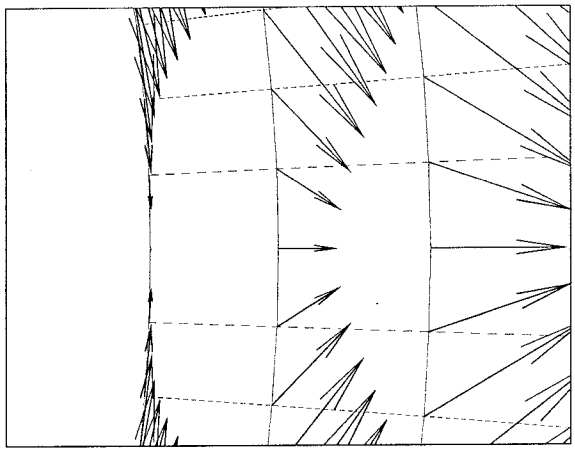

**Figure 12.** Relative Velocity Vectors at the Trailing Stagnation Point of the Cylinder.

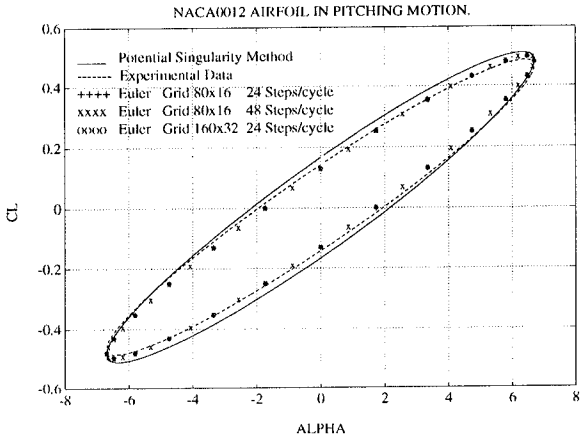


**Figure 13.** Calculation of a NACA0012 Airfoil in Pitching Motion. Amplitude $\Delta\alpha = \pm 6.7°$, Reduced Frequency $k_c$=0.4, Pitching Axis $a = -0.13$.